



Cite this: *Phys. Chem. Chem. Phys.*,
2017, **19**, 32617

Effects of the c-Si/a-SiO₂ interfacial atomic structure on its band alignment: an *ab initio* study†

Fan Zheng, Hieu H. Pham and Lin-Wang Wang*

The crystalline-Si/amorphous-SiO₂ (c-Si/a-SiO₂) interface is an important system used in many applications, ranging from transistors to solar cells. The transition region of the c-Si/a-SiO₂ interface plays a critical role in determining the band alignment between the two regions. However, the question of how this interface band offset is affected by the transition region thickness and its local atomic arrangement is yet to be fully investigated. Here, by controlling the parameters of the classical Monte Carlo bond switching algorithm, we have generated the atomic structures of the interfaces with various thicknesses, as well as containing Si at different oxidation states. A hybrid functional method, as shown by our calculations to reproduce the GW and experimental results for bulk Si and SiO₂, was used to calculate the electronic structure of the heterojunction. This allowed us to study the correlation between the interface band characterization and its atomic structures. We found that although the systems with different thicknesses showed quite different atomic structures near the transition region, the calculated band offset tended to be the same, unaffected by the details of the interfacial structure. Our band offset calculation agrees well with the experimental measurements. This robustness of the interfacial electronic structure to its interfacial atomic details could be another reason for the success of the c-Si/a-SiO₂ interface in Si-based electronic applications. Nevertheless, when a reactive force field is used to generate the a-SiO₂ and c-Si/a-SiO₂ interfaces, the band offset significantly deviates from the experimental values by about 1 eV.

Received 28th August 2017,
Accepted 13th November 2017

DOI: 10.1039/c7cp05879a

rsc.li/pccp

I. Introduction

Amorphous oxides are often used as insulating, protecting or carrier stopping layers for many electronic and optoelectronic applications. In such applications, the electronic structure of the system, *e.g.*, the band alignment between the oxides and the underlying crystal substrate and the possible interfacial electronic states, are of high interest. Although density functional theory (DFT) interface studies have become quite common and are often complemented by high-level methods such as band gap corrections, it is still relatively rare to find theoretical amorphous–crystal interface studies. This does not mean the crystal/amorphous interface is not important. Quite the contrary; such interfaces exist in the majority of electronic applications. The main reason for the lack of theoretical study is the difficulty of constructing the reliable atomic structure of the interface and testing such structures against experiments once the structure has been constructed. Furthermore, unlike the crystal/crystal interface,

the crystal/amorphous interface often requires large supercells, which makes the calculation much more expensive. However, with advances in computing power and computational algorithms, we can now calculate systems consisting of a few hundred atoms and use methods like the hybrid functional, which has the potential to describe the electronic structure more accurately than the local or semilocal functionals, such as local density approximations (LDAs) or generalized gradient approximations (GGAs). The new applications of the amorphous oxide insulating or protection layer, *e.g.*, in solar cells or solar electric chemical cells, and the push for a more fundamental understanding of their carrier dynamics, raise renewed interest in these systems. In this work, we use c-Si/a-SiO₂ as an example to study such a crystal/amorphous interface. In particular, we compare different interfacial atomic structures and their electronic structure consequences. From such a comparative study, we can estimate both the reliability of the different procedures to construct the atomic structure and the physical understanding of different interfaces.

The c-Si/a-SiO₂ interface is ubiquitous in Si-based electronic devices. It is one of the most well-studied crystal–amorphous interfaces due to its predominance in electronic applications.^{1–16} Besides being used in CMOS technology, it is also widely used in other applications. For example, in photoelectrochemistry, amorphous SiO₂ has been one of the most popular protective

Joint Center for Artificial Photosynthesis and Materials Sciences Division,
Lawrence Berkeley National Laboratory, Berkeley, California 94720, USA.
E-mail: lwwang@lbl.gov

† Electronic supplementary information (ESI) available. See DOI: 10.1039/c7cp05879a

layers to protect the light absorber, such as Si, from being corroded by the electrolyte or water.¹⁷ The current engineering techniques can tune the thickness of the SiO₂ film to as small as 0.6 nm, in order to improve the gate capacitance in the metal-oxide-semiconductor capacitor, or to enhance the hole tunneling transport in a silicon photoanode.¹⁸ With such thin SiO₂, the details of the interface with Si become extremely important. Different synthesizing and oxidation procedures might produce different interfacial atomic structures. Understanding the influence of the interfacial atomic structure on the electronic structure of the system is therefore of great significance. In the late 1980s, there was a burst of theoretical studies on c-Si/a-SiO₂. These studies yielded band offsets in agreement with experiments. However, most of these studies were based on relatively small supercell systems; in particular, for *ab initio* calculations. Often, only one atomic structure was used, and there was no systematic comparison of different atomic structures. Moreover, most previous theoretical studies were based on LDA/GGA, with estimated postprocessing corrections to the LDA/GGA band gap error. In the current work, we use different strategies to construct the crystal/amorphous interface, and compare different interfacial atomic structures. We also use the hybrid functional (HSE) to directly calculate the whole system without the need for further postprocessing corrections.

It is well known from early studies that one predominant feature of the c-Si/a-SiO₂ interface is its relative abruptness in the interfacial layers, as is shown in TEM images.¹⁷ Nevertheless, the interface can extend beyond one monolayer to two or three atomic monolayers.^{19–22} An even more extensive transition layer larger than 10 Å has been identified using X-rays.^{8,23} Within the transition region, photoemission and photoelectron spectroscopies demonstrate the presence of the suboxide layer,^{20,21,24} composed of Si with oxidation states of Si¹⁺, Si²⁺ and Si³⁺. Further measurements show their ratio to be 1:2:3 or 1:2:1 depending on the synthesis conditions.^{25,26} Meanwhile, molecular dynamics (MD) using a reactive force field^{5,27} and Monte Carlo (MC)²⁸ simulations have also shown the existence of an interfacial layer beyond 10 Å. Owing to their relatively small computational costs, different valence force fields have been used to study both bulk a-SiO₂ and its interface with Si.^{29,30} The band gap and band offset were mainly computed using an LDA or GGA method. However, the LDA/GGA methods do not always show agreement with the experimentally measured band offset due to the well-known issue of band-gap underestimation. As a result, further corrections such as *GW* and hybrid functionals have been used to correct the LDA/GGA band gaps, showing good agreement with experiments.^{31–33} However, as far as we know, there has been no systematic study of the electronic structures of different interfacial atomic structures; in particular, using the methods of electronics structure calculation (*e.g.*, the hybrid exchange–correlation functional) without postprocessing corrections directly.

As illustrated in both experimental and theoretical work, the size of the transition regions spans a broad range. As a result, the thickness of the interface is non-negligible compared with the thickness of the SiO₂ layer for thin SiO₂ layer applications. Therefore, understanding the effect of the transition region on

the electronic structure of the interface is of great interest. In this study, *via* bond switching (BS) MC simulations, the thickness of the transition region was measured by the maximum number of Si atoms connected *via* continued Si–Si bonds starting from the fixed crystal Si region. The band offset was computed using the hybrid functional method. A special technique was developed, which allows the application of a regional mixing parameter to the hybrid functional, hence enabling the band gaps of both the Si and SiO₂ regions to be described accurately. Our results show excellent agreement with the experimental band offset, and also reveal the robustness of the band offset to the detailed interfacial atomic profile.

II. Calculation methods

A. Monte Carlo simulations

A continuous random network, or say the BS MC simulation, has been demonstrated to be an effective way to generate the amorphous structures of covalent bonding materials.^{34–37} During the BS procedure, a pair of nearby bonds (either Si–Si or Si–O type bonds) is selected. This pair of bonds, A–B and C–D, are switched into a new pair of bonds: A–C and B–D. By enforcing the new bond topology into the valence force field (VFF), the switched atomic structure is fully relaxed. The total energy of the relaxed structure is compared with the previous step, and this new structure is accepted or rejected following the Metropolis MC scheme. Many sophisticated force fields, such as Tersoff and its derivatives,^{38–41} Yasukawa,⁴² and Stillinger–Weber⁴³ potentials have been applied to studies of the Si/SiO₂ interface. However, many of such force fields are designed to break the bond, which does not apply to the continuous random network scheme. The VFF as the simplest one is capable of describing the structure well, and it is straightforward to implement it into the BS MC scheme. In our simulation, the following VFF⁴⁴ was used to relax the structure.

$$E_{\text{tot}} = \frac{1}{2} \sum_i k_b (d_i - d_0)^2 + \frac{1}{2} \sum_{i,j} k_\theta (c_{ij} - c_0)^2 + U_{\text{repulsion}} \quad (1)$$

where $k_{b,\text{Si-O}} = 27 \text{ eV } \text{\AA}^{-2}$, $k_{b,\text{Si-Si}} = 9.08 \text{ eV } \text{\AA}^{-2}$, $k_{\theta,\text{Si-O-Si}} = 0.75 \text{ eV}$, $k_{\theta,\text{O-Si-O}} = 4.32 \text{ eV}$, $k_{\theta,\text{Si-Si-Si}} = 3.58 \text{ eV}$, $k_{\theta,\text{Si-Si-O}} = (k_{\theta,\text{Si-Si}} k_{\theta,\text{O-Si-O}})^{1/2} \text{ eV}$, and d_0 and c_0 are taken from the DFT relaxed Si and SiO₂. The last term $U_{\text{repulsion}} = \frac{1}{2} \sum_{(i,j)} k_r (d_{ij} - d_{\text{neighbor}})^4$ when

$d_{ij} < d_{\text{neighbor}}$ is to avoid the overlap of two atoms that are not directly connected by a bond. k_r is set to be 1 eV \AA^{-4} . d_{neighbor} is taken differently depending on the two neighboring atomic species ($d_{\text{neighbor, Si-O}} = 3.2 \text{ \AA}$, $d_{\text{neighbor, O-O}} = 2.58 \text{ \AA}$, and $d_{\text{neighbor, Si-Si}} = 3.84 \text{ \AA}$). This term turns out to be important for obtaining a reasonable structure, in particular near the interface.^{29,30,34} By taking the derivative of the total energy to the atomic position, the force can be derived. With the total energy and the force as inputs, the conjugate-gradient minimization scheme is used to relax the structure. Since MC simulations are used to obtain the bond topology for the amorphous structure, the accuracy of the relaxation is not crucial, and we set the force threshold to be 0.3 eV \AA^{-1} .

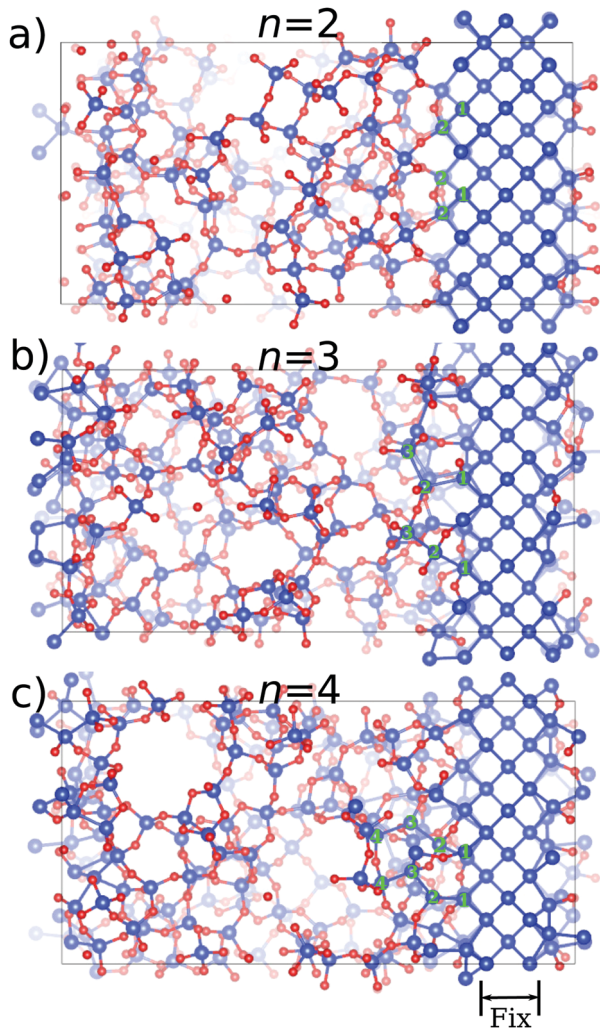


Fig. 1 DFT relaxed structures reported from the MC simulations. Here, different maximum numbers of Si atoms (n) connected via the continued Si–Si bonds are used to represent the thickness of the transition region: (a) $n = 2$, (b) $n = 3$, and (c) $n = 4$. The green digits are used to count the Si atoms, which are connected by continued Si–Si bonds spreading from the fixed Si atoms as examples. The middle three Si layers are fixed in the MC simulations and DFT relaxation. The Si–Si bonds connected to these fixed atoms are not allowed to switch during the MC simulations.

The middle three layers of Si and their bonds are fixed in order to maintain the crystalline structure of Si (Fig. 1). However, if all other Si atoms are allowed to participate in the bond switch, it is easy to form Si–Si bonds extended to the SiO_2 regions. These Si–Si bonds cause suboxide layers with Si^{1+} , Si^{2+} , and Si^{3+} oxidation states. In order to quantify the thickness of this suboxide layer, we count the maximum number (n) of Si atoms connected via the continued Si–Si bonds starting from the fixed Si atom layer (Fig. 1). In our BS MC procedure, we deliberately limit n to be 2, 3 and 4 (e.g., to make a $n = 3$ suboxide layer; if n is larger than 3 during MC simulations, the bond switch will be rejected) to generate different interfacial thicknesses. This allows us to have a systematic procedure to produce and thoroughly study different transition layers at various thicknesses. Here, $n = 2$ corresponds to the “abrupt”

interface with only one layer of atoms for the transition region, which has two Si–O bonds and two Si–Si bonds. Such an abrupt interface is interesting since this is the case for most of the c-Si/c- SiO_2 interfaces constructed in many theoretical studies. It is interesting to note that it is possible to have such an interface in the c-Si/a- SiO_2 interface structure. During the MC simulation, following previous literature studies, the first $N/2$ steps, *i.e.* BS steps, are all accepted to fully amorphize the crystal at the beginning (N is the number of atoms in the simulation cell). Then, stimulated annealing at a very high temperature (10,000 K) is used to cool the structure and reduce the local strain. During cooling, a new temperature is set as 70% of the previous temperature step, and a total of around 300 000 BS MC steps are performed to reach equilibrium.

B. Reactive force field MD simulations

We also used MD simulations and a “melt-and-quench” technique to obtain c-Si/a- SiO_2 along the [001] direction using a reactive force field (ReaxFF)⁴⁵ approach. More specifically, the interatomic interactions between the Si–Si, Si–O and O–O pairs were characterized using the ReaxFF, which has been shown to reproduce well the structural properties of crystalline SiO_2 . During the molecular dynamics simulations, the Si part was kept frozen and the SiO_2 part was first heated up to a high temperature until the crystals completely lost their structural memory. This was then equilibrated for a short period at this temperature (for 5 ps at 3500 K), followed by slowly cooling to room temperature over 100 ps, which allowed the formation of the SiO_2 amorphous phase. The time step for the MD simulations was 0.5 fs and a canonical ensemble (*NVT*, constant volume and constant temperature) was used. Here, we followed the same procedure as employed by Kovacevic *et al.* for our MD simulation.⁴⁶

C. Electronic structure calculations

The plane-wave package PWmat^{47,48} was used to relax the DFT atomic structure and compute the electronic properties, using a GGA exchange–correlation functional.⁴⁹ PWmat produces essentially the same results as Quantum Espresso,⁵⁰ but with efficient GPU accelerations. The norm-converging pseudopotential was used with a wavefunction energy cutoff of 50 Ryd with a single Γ -point.⁵¹ In order to obtain the band offset, the last few snapshots from the end of the MC simulations were fully relaxed using DFT until all the components of the forces were below 0.05 eV Å^{−1}. The local density of states were then computed to reveal the layer-resolved band energies along the direction perpendicular to the interface in order to illustrate the band offset.

However, such a band offset obtained from the GGA suffers from the underestimation of the band gap. A hybrid functional that includes the exact exchange integral has been shown to improve both the band gaps of bulk materials and the band offsets of heterostructures.⁵² Furthermore, the exact amount of exchange represented by a mixing parameter, α , is inversely proportional to the high-frequency dielectric constant of the material (ϵ_∞).⁵³ Thus, in theory, the mixing parameters for the small band gap Si and the large band gap SiO_2 should be different.

Indeed, this is true in practice. In our PWmat calculation using the norm-conserving pseudopotentials, we found that a mixing parameter of 0.15 was needed for crystal Si, and 0.35 was needed for crystal SiO_2 in order to yield their perspective band gaps of 1.12 and 8.5 eV. To solve this problem, we introduced an atomic specific mixing parameter. More specifically, an atom-weighted mask function $f(\mathbf{r}) = 1 + \sum_i a_i e^{-(\mathbf{r}-\mathbf{R}_i)^2/\sigma^2}$ was introduced with a_i as an atomic specific parameter for the atom i and \mathbf{R}_i as the atomic position. Then, the exchange interaction in the total energy expression could be written as:

$$\sum_{i,j} 0.25 o(i)o(j) \int \int \psi_i(\mathbf{r}) \psi_j^*(\mathbf{r}) f(r) \frac{\operatorname{erfc}(\omega(\mathbf{r} - \mathbf{r}'))}{|\mathbf{r} - \mathbf{r}'|} f(r') \psi_i^*(\mathbf{r}') \psi_j(\mathbf{r}') d^3 r' d^3 r'$$

where $\psi_i(\mathbf{r})$ are the wave functions, and $o(i)$ is its occupation number. The prefactor 0.25 is the original mixing parameter in the HSE. The local part of the GGA exchange energy density will also been modified by a factor of $1 - 0.25f(r)$.² By setting a_i for each atom type, an effective local mixing parameter can be achieved. We determined the a_i parameters by requiring the hybrid functional to reproduce the experimental crystal Si and bulk amorphous SiO_2 band gaps as $a_{\text{Si,Silicon}} = -0.1$ and $a_{\text{Si,O;SiO}_2} = 0.24$. As is demonstrated below, by implementing this method, the appropriate band offset could be obtained through a self-consistent hybrid functional calculation, which should provide more reliable electronic structures and wave function localizations than postprocessing corrections. Here, all the HSE calculations were carried out using the PWmat code, which has a fast scheme to calculate the HSE. For our 513-atom supercell system, with 2592 electrons and an energy cutoff of 50 Ryd, the self-consistent HSE calculation requires about 4 hours using eight GPUs.

III. Results and discussion

A. Structure of the interface

To validate the effectiveness of the VFF and the BS MC method, we tested our procedure by first building amorphous bulk SiO_2 with 243 atoms. Fig. 2 shows the calculated radial distribution function (RDF) for the systems prepared by BS MC and ReaxFF MD, compared with the experimental values.⁵⁴ From this graph, we can see that the BS MC method reproduces not only the peaks for short-range radii but also the main peaks for a distance of more than 5 Å, demonstrating its validity in describing the amorphous features of SiO_2 . For ReaxFF MD, although it predicts the first peak (Si-O bond) correctly, it deviates significantly from the experimentally measured second peak (O-O distance), which may be caused by the lack of accuracy for the O-Si-O angle description. This can be further shown in Fig. 2b, where the O-Si-O angle distributions of BS MC and ReaxFF MD amorphized structures are compared. As expected, most of the angles from the BS MC simulation are around 109.5° , corresponding to the tetragonal cage of Si and O. However, the angles of the structure from the ReaxFF MD sample a broad range from 87° to 143° . In particular, the small angles around 90° correspond to a significantly underestimated value (2.3 Å) for the O-O distance in the RDF.

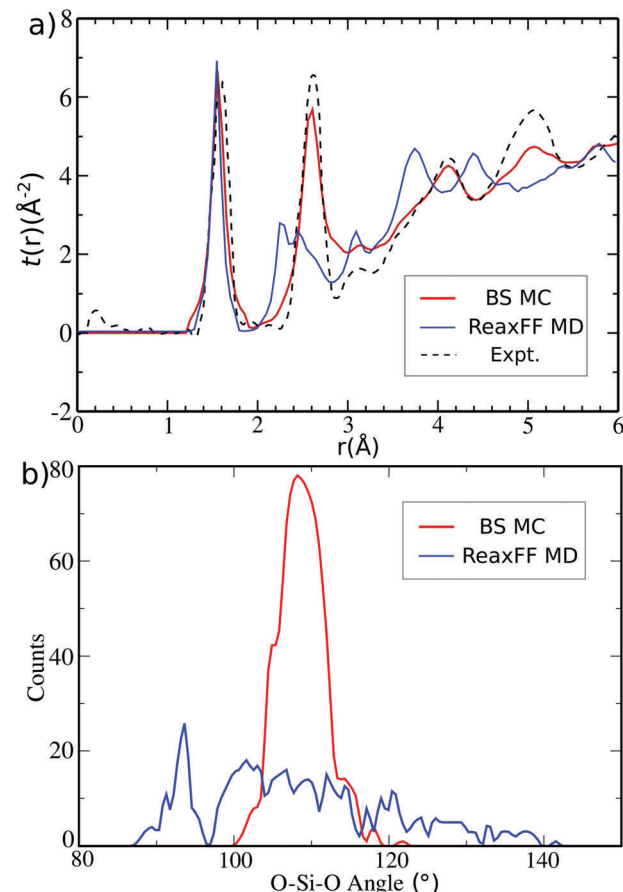


Fig. 2 (a) Radial distribution function (RDF) comparison with BS MC, ReaxFF MD and experimental values. (b) O-Si-O angle distribution histogram of the structures from BS MC and ReaxFF MD.

With this confidence, we continued to explore the c-Si/a- SiO_2 interface using the BS MC simulation. The initial structure was constructed by stacking the crystalline SiO_2 on Si along the [001] direction, albeit with significant strain on the crystalline SiO_2 . Here, the supercell $3 \times 3 \times 2$ of the cubic Si was used for the Si part of the interface with the a - and b -axis fixed to be the lattice constant of the Si crystal. The length of the c -axis of the supercell was determined based on the experimental density of amorphous SiO_2 .^{29,55} This initial structure was fully relaxed to relieve the local strain at the interface with its resulting configuration as our initial atomic structure of the BS MC algorithm. This was followed by the BS MC simulation with the procedure to control the interface thickness as described above. The last few snapshots from the MC simulations were used for DFT relaxations, and the resulting structures with different thicknesses of the transition regions were obtained and are shown in Fig. 1. For all the structures with different interface thicknesses n , the SiO_2 part was fully amorphized. When $n = 2$, there was only a single atomic layer in the transition region, which mainly contained Si^{2+} atoms. As n increased to 3 and 4, we noticed the continued Si-Si bonds spreading into the SiO_2 part (Fig. 1), forming all five oxidation states of Si. Meanwhile, the number of layers containing suboxide Si atoms increased from

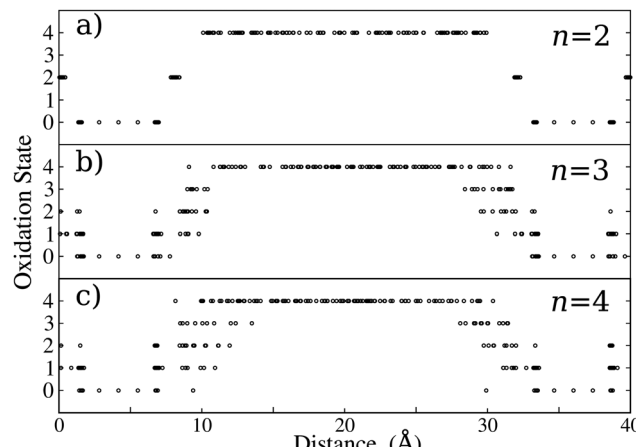


Fig. 3 The oxidation states of Si atoms averaged for a given distance along the [001] direction for the whole supercell under different n values.

a monolayer to several atomic layers, expanding the transition regions.

Such expansion of the transition region can be further indicated by the characterization of the Si suboxide with its oxidation state determined by the number of bonded oxygen atoms. Fig. 3 shows the distribution of the oxidation states of Si along the [001] direction under different thicknesses n . Although Si only showed the 0 and 4+ oxidation states deep inside the Si and SiO_2 regions, the suboxide Si became dominant near the interface. For example, the $n = 2$ structure showed the thinnest transition region, which occupied only a single atomic layer (around 3 Å). As n increased to 3 and 4, the transition region spanned more layers, extending up to 5 Å and 8 Å, respectively. Furthermore, the ratio of this suboxide Si could be counted. In the case of $n = 2$, the ratio of the 1+, 2+ and 3+ states was distributed as 0 : 1 : 0 across the transition region. For $n = 3$ and $n = 4$, this ratio turned out to be 1 : 1.08 : 0.84 and 1 : 0.74 : 0.66, respectively. We can see that the thicker interface had more variety of Si valence states. The reported experimental values of this ratio vary widely, *e.g.* 1 : 2 : 3 in ref. 25, and 1 : 2 : 1 in ref. 26. The ratio might depend sensitively on the synthesis conditions or the experimental probing techniques. At this point, it is difficult to make a quantitative comparison with any specific experiments. We find that the valence states of Si are in roughly similar orders between the 1+, 2+ and 3+ states in the $n = 3$ and 4 interfaces. Thus, these experimental interfaces might not be the abrupt interface as illustrated in the $n = 2$ case.

B. Electronic structures

The band gap of the interface is controlled by the band gap of the Si part, which is around 1.1 eV. Considering the $n = 2$ structure as an example, Fig. 4 shows the local density of states (LDOSs) summed for the Si crystal part (Si^0), the amorphous SiO_2 part (Si^{4+} and O) and the transition part (Si^{2+}), calculated using the local parameterized HSE functional. As is shown by the density of states, the states near the band gap are dominated by the Si atoms inside the Si layer, without any defect states in the band gap. To show this more clearly, we plotted the

wavefunction in real space for the conduction band minimum (CBM) and valence band maximum (VBM) as illustrated in Fig. 4b and c. This clearly shows that the wavefunctions are well localized inside the crystal Si. As for the Si atoms in the transitional region, although they form only one atomic layer, their energies spread broadly for both low energy near the band gap (Si-like) and high energy away from the band gap (SiO_2 -like). This may be due to their mutual bonds with Si and O atoms. However, the energies of the Si^{4+} atoms are pushed far away from the band gap by Si-O bonding, featuring the SiO -like band energies.

The calculated LDOS was also used to estimate the “local” electronic structure and the band offset of the c-Si/a- SiO_2 interface. This was performed by averaging over the LDOS of the atoms within a given distance range along the [001] direction. Fig. 5a illustrates the GGA computed energies of the CBM and VBM along the [001] direction for the $n = 2, 3$ and 4 structures. The valence and conduction band offset (VBO and CBO) can be

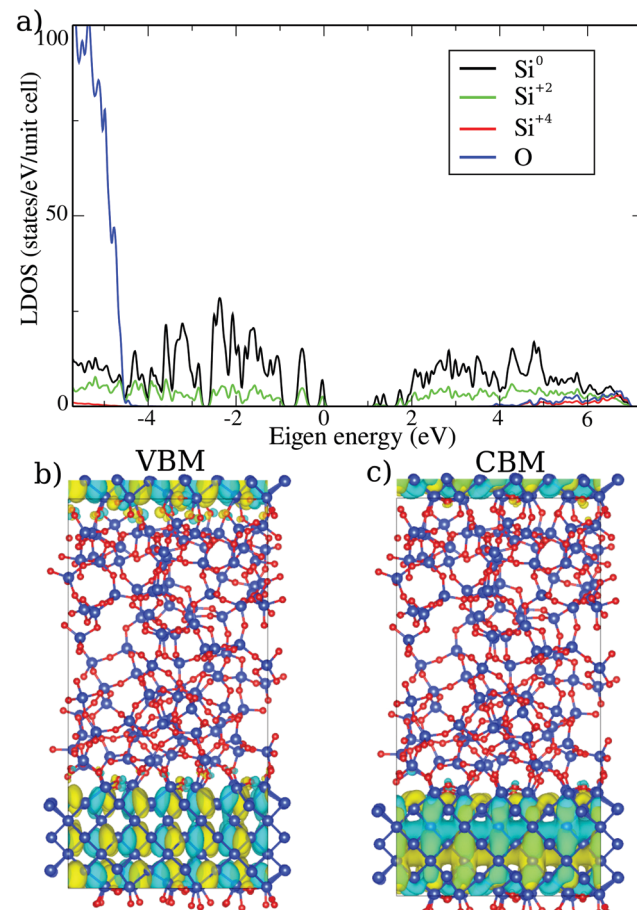


Fig. 4 (a) The HSE calculated local density of states for Si^0 atoms (the Si-bulk part), Si^{2+} (the transition region), Si^{4+} (the SiO_2 -bulk part) and O (the SiO_2 -bulk part) atoms obtained from the $n = 2$ structure. Here, the Si^{4+} and O atoms are from the middle of the SiO_2 -bulk part to exclude the contribution from the interfacial region. 0 energy is set to be at the valence band maximum. Real space wavefunction isosurface for the (b) valence band maximum (VBM) and (c) conduction band minimum (CBM) of this structure.

computed from the energy difference between the SiO_2 and Si parts, *i.e.* $\text{VBO} = \text{Max}[\text{VBM}_{\text{Si}} - \text{VBM}_{\text{SiO}_2}]$ and $\text{CBO} = \text{Max}[\text{CBM}_{\text{SiO}_2} - \text{CBM}_{\text{Si}}]$. For all the structures with different n that we calculated, the CBO values were around 1.8 eV, and the VBO values were 2.5 eV, which is consistent with other theoretical studies.^{7,52}

Our results, as shown in Fig. 5, are a bit counter-intuitive. For the $n = 2, 3$, and 4 cases, the amount of fixed bulk Si regions is the same. Intuitively, one expects that the band offset starts at the same place from the bulk Si edge, and the thicker interfacial layer case of $n = 4$ should have a wider band offset turn-on region, just like the Si oxidation profile shown in Fig. 3. However, Fig. 5 shows that the band edge transition areas for $n = 2, 3$, and 4 have similar thicknesses (sharpness). Furthermore, the bulk Si-like band edge has been pushed out for the $n = 4$ case from the structurally bulk Si region. As a result, the effective bulk SiO_2 region for the $n = 4$ case is much shorter, while the electronic transition areas measured from LDOS are

the same for $n = 2, 3$, and 4. This will have a significant consequence for the insulating capability and tunneling transport for the $n = 4$ case, particularly when the SiO_2 layer is thin. The reason for the push out of the Si bulk state into the transition area is that, whenever there are Si-Si bonds, linking directly from the bulk Si area, the CBM and VBM wave functions will be extended to those Si atoms, even though these Si atoms are already partially oxidized as they also form Si-O bonds. This can be directly visualized from the real space wavefunctions for the band edges. Fig. 5b and c show the wavefunctions for the CBM and VBM of the $n = 3$ and 4 structures. Together with the $n = 2$ case (Fig. 4b), these Si atoms in the SiO_2 part, though partially oxidized, still contribute to the band edge states. Also due to this contribution, as well as local strains caused by the thicker interface, the VBM and CBM wavefunction isosurfaces look more disordered in Fig. 5b and c even in the region of c-Si for $n = 3$ and 4 compared with the case of $n = 2$, as shown in Fig. 4b and c.

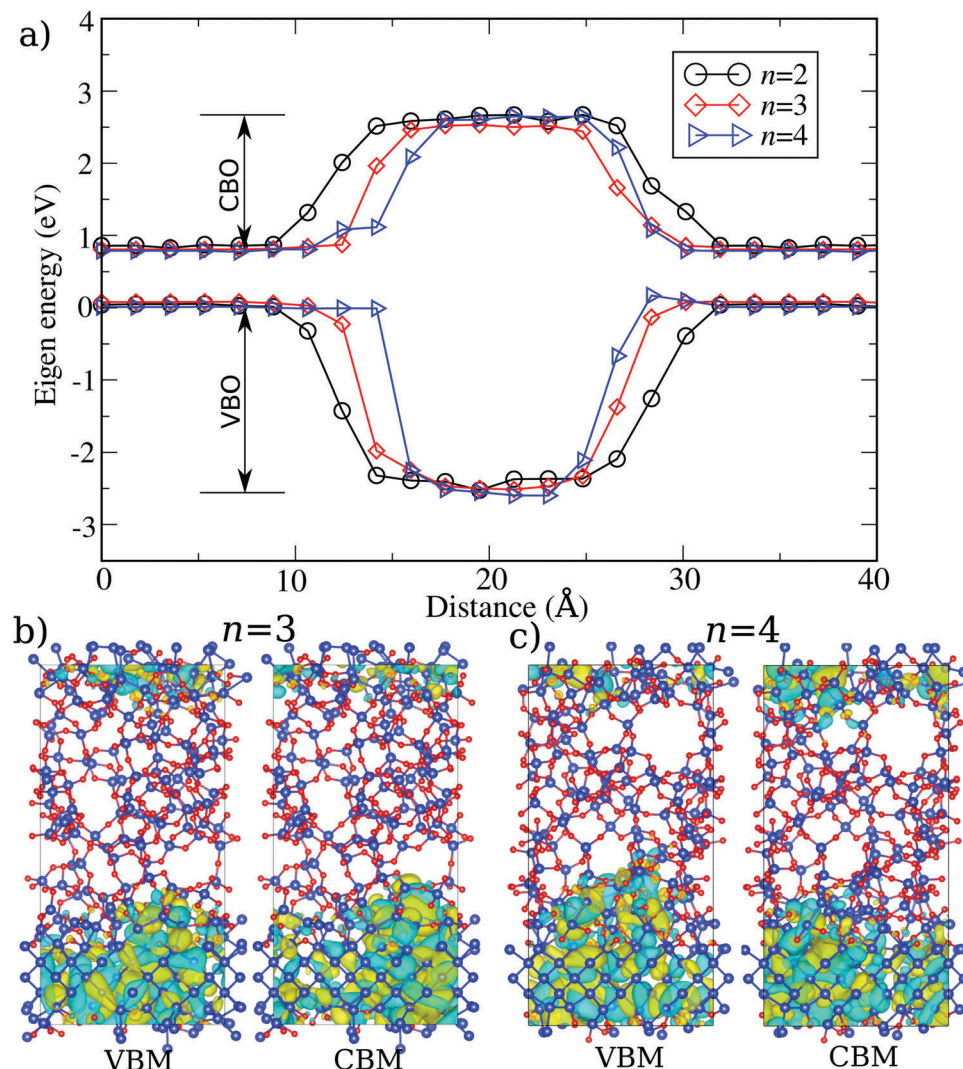


Fig. 5 (a) The GGA calculated VBM and CBM averaged for a given distance along the [001] direction across the interface for structures with $n = 2, 3$ and 4. The left and right ends correspond to the Si-bulk part, with 0.8 eV band gap; the middle part corresponds to the SiO_2 -bulk part, with around 5.2 eV band gap. The valence band offset is computed as 2.5 eV, and the conduction is 1.8 eV. (b) The VBM and CBM wavefunctions in real space for the structures with $n = 3$ and 4.

The second significant finding of our simulation is that the magnitudes of the band offsets are independent of the interfacial transition layer thickness. As shown from this graph (Fig. 5), the thickness of the transition region does not affect the value of the band offset significantly. Although different n values show quite different “local” band gaps near the transition region, the overall band offset is still determined by the states inside the Si and SiO_2 parts, unrelated to the details of the transition region. This means the band offset is not driven by an interfacial dipole moment, since such a dipole moment should depend on the details of the transition layer. Instead, the intrinsic band positions of the bulk Si and SiO_2 determine the band alignment. It is possible that the random nature of the amorphous structure allows the system to avoid the large interfacial dipole moment. It remains to be seen if this is generally true of the crystal/amorphous band alignment.

As mentioned above, the different mixing parameter α can be assigned to atoms locally. In order to obtain the appropriate α for Si and SiO_2 , we evaluated the band gaps calculated by different α for crystalline Si and amorphous SiO_2 as shown in Fig. 6a and b, respectively. For the amorphous SiO_2 , a 243-atom bulk structure ($3 \times 3 \times 3$ supercell) was used, generated by the same BS MC simulation procedure and relaxed by a GGA, which is large enough to represent the SiO_2 part in the interface. From the linear relation of the band gap and a_i , the value of a_i can be easily obtained to reproduce the experimental band gap. We chose $a_i = -0.1$ for Si at the pure Si region, and 0.24 for Si and O in the amorphous SiO_2 region. We employed this newly developed hybrid functional calculation method and computed the band offsets as shown in Fig. 6c for the structures with $n = 2, 3$ and 4. From this graph, the HSE-calculated band offsets display excellent agreement with the experiments, demonstrating the validity of the BS MC scheme and the newly developed HSE method. Besides the band offset, the HSE calculated results show similar features (e.g., the band edge wave functions) to the results calculated by the GGA method as discussed above. All the structures tend to have a unified band offset, which is unrelated to the thickness of the transition regions. Similar to the GGA calculations, the bulk Si-like band edge has been pushed into the SiO_2 region for the structures with “thick” transition regions. Here, we want to emphasize that our HSE method does not need postprocessing corrections to the Si or SiO_2 separately, which provides a consistent description of the charge density, wavefunction and potential of the interface. These quantities can be used for further analysis such as charge transfer crossing the interface. However, we do note that, in the above, the local density of state (LDOS) was used to determine the band offset. This could include the quantum confinement effect due to the small thickness of the c-Si layer. A common way to avoid such a quantum confinement effect is to use a local potential profile instead of LDOS. However, the LDOS determined band gap for the Si region is about 1.1 eV, which is similar to the result of the HSE bulk Si band gap. This indicates that the quantum confinement effect in this system is relatively small. This is probably because the Si effective masses of both the conduction band in the Γ -X direction, and the valence band heavy hole, are rather large.

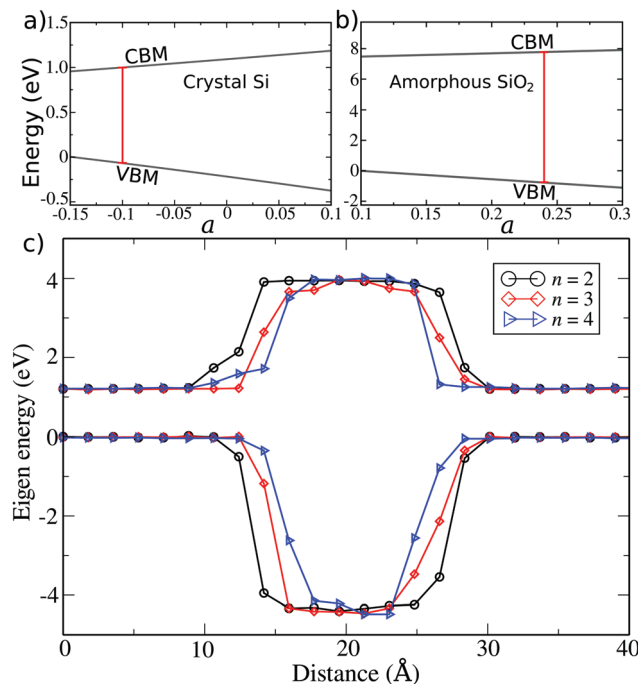


Fig. 6 (a) CBM and VBM energies of the silicon crystal calculated by a different mixing parameter α of the HSE. Here, α is adjusted by a as described in the Methods section. (b) VBM and VBM energies of the 243-atom amorphous SiO_2 with different α values. (c) HSE calculated band offset of the structure for the structures with $n = 2, 3$ and 4.

As mentioned above, we also calculated the band offset of the structure prepared by the ReaxFF MD simulation. By considering the snapshots out of the MD trajectory after equilibration, the electronic structure and band offset of the a- SiO_2 /c-Si interface were calculated using the GGA. The direct structure prepared by MD simulated annealing usually has one or two defect states due to an imperfect bonding topology. However, a small number of hydrogen atoms can be used to compensate the dangling bonds at those defect sites to eliminate the in-the-gap defect states. The band gap and the CBO and VBO values obtained from GGA calculations were 0.76, 2.92 and 2.06 eV, respectively. It is also shown that both the CBM and VBM come from the Si part, which suggests a straddling type of band alignment similar to the BS results (Fig. 5). As a summary, Table 1 summarizes the calculated band offsets from BS MC and ReaxFF MD simulations. Since the GGA calculated ReaxFF CBO is 1 eV higher than the results of the BS MC simulation, this indicates that the GGA band corrected band offset would be 1 eV off from that of the experimental results. Such a deviation using the ReaxFF MD simulation may arise from the less accurate O-Si-O angle description as well as the dangling bonds emerging during the MD. Although ReaxFF allows one to simulate the process of bond breaking and bond formation, which is quite relevant for the formation of the amorphous structure in this case, the final structure would be subject to how the force fields were trained, typically against DFT-derived energies as well as the simulated annealing procedure. Nevertheless, if an accurate ReaxFF is obtained and sufficient simulation time is

Table 1 Conduction and valence band offsets (eV) computed by ReaxFF MD, BS MC, and the HSE corrected BS. Other computational work with GGA or LDA and the experimental results are listed for comparison

	ReaxFF	BS	BS-HSE	Other work (GGA/LDA)	Expt.
Conduction band offset	2.9	1.8	2.9	1.8, ⁷ 2.3 ⁵²	3.0 ⁵⁶
Valence band offset	2.1	2.5	4.4	2.5, ⁷ 2.5 ⁵²	4.3 ⁵⁷

possible, the ReaxFF can be used to simulate the actual synthesis process, which is missing in the BS MC method. In contrast, BS MC using the VFF conserves the bonding orders to avoid the dangling bond. Thus, by design, the BS MC gives better covalent bonding topology, leading to less defects. This, however, also lacks some real situations such as the bonding defects in reality. In practice, we found that the BS MC provides a better amorphous structure in our calculation.

IV. Conclusion

Although the crystalline Si/amorphous SiO₂ interface is widely used for numerous applications, its band offset dependence on the thickness of the transitional region was not fully explored. In this study, by performing bond switching Monte Carlo simulation and first-principle calculations, we have studied the band offset of the crystalline Si/amorphous SiO₂ interface under different thicknesses of the transitional region. For these structures with different thicknesses, we find that, although the detailed atomic structures near the interface differ significantly, the band offsets of all the different thicknesses tend to be the same. On the other hand, the bulk Si band-edge feature has been extended into the transition area, which leads to a smaller effective SiO₂ region. Our calculation shows that the band offset is rather robust to the details of the transition layers. This is a major advantage for electronic devices because it can reduce the device variation, which is a major issue when the device length shrinks to the nano size. As a comparison, we also performed a reactive force field molecular dynamics simulation to construct the interface. The calculated band offset shows that the bond switching method tends to give results that are more consistent with experiments, both for the atomic structure and the electronic band offset. Moreover, by applying the newly developed hybrid functional with atomic specific mixing parameters, we can correct the band gaps of Si and amorphous SiO₂ simultaneously using one heterostructure calculation, and thus it can be used for future studies on transport and defect state carrier localizations.

Conflicts of interest

There are no conflicts to declare.

Acknowledgements

This material is based on work performed by the Joint Center for Artificial Photosynthesis, a DOE Energy Innovation Hub,

supported through the Office of Science of the U.S. Department of Energy under Award number DE-SC0004993. We used the resources of the National Energy Research Scientific Computing Center (NERSC) located in Lawrence Berkeley National Laboratory.

References

- 1 S. C. Witczak, J. S. Suehle and M. Gaitan, *Solid-State Electron.*, 1992, **35**, 345.
- 2 A. C. Diebold, D. Venables, Y. Chabal, D. Muller, M. Weldon and E. Garfunkel, *Mater. Sci. Semicond. Process.*, 1999, **2**, 103.
- 3 A. Stesmans and V. V. Afanas'ev, *J. Phys.: Condens. Matter*, 1998, **10**, L19.
- 4 Z. H. Lu, M. J. Graham, D. T. Jiang and K. H. Tan, *Appl. Phys. Lett.*, 1993, **63**, 2941.
- 5 D. A. Muller, T. Sorsch, S. Moccio, F. H. Baumann, K. Evans-Lutterodt and G. Timp, *Nature*, 1999, **399**, 758.
- 6 S. Dumpala, S. R. Broderick, U. Khalilov, E. C. Neys, A. C. T. van Duin, J. Provine, R. T. Howe and K. Rajan, *Appl. Phys. Lett.*, 2015, **106**, 011602.
- 7 F. Giustino, A. Bongiorno and A. Pasquarello, *J. Phys.: Condens. Matter*, 2005, **17**, S2065.
- 8 S. D. Kosowsky, P. S. Pershan, K. S. Krisch, J. Bevk, M. L. Green, D. Brasen, L. C. Feldman and P. K. Roy, *Appl. Phys. Lett.*, 1997, **70**, 3119.
- 9 F. Giustino and A. Pasquarello, *Phys. Rev. Lett.*, 2005, **95**, 187402.
- 10 T. Watanabe, *Jpn. J. Appl. Phys.*, 1999, **38**, L366.
- 11 D. Fischer, A. Curioni, S. Billeter and W. Andreoni, *Appl. Phys. Lett.*, 2006, **88**, 012101.
- 12 Z. Huiwen, L. Yongsong, M. Lingfeng, S. Jingqin, Z. Zhiyan and T. Weihua, *J. Semicond.*, 2010, **31**, 082003.
- 13 A. Pasquarello, M. S. Hybertsen and R. Car, *Phys. Rev. Lett.*, 1995, **74**, 1024.
- 14 A. Pasquarello, M. S. Hybertsen and R. Car, *Phys. Rev. B: Condens. Matter Mater. Phys.*, 1996, **53**, 10942.
- 15 T. Yamasaki, C. Kaneta, T. Uchiyama, T. Uda and K. Terakura, *Phys. Rev. B: Condens. Matter Mater. Phys.*, 2001, **63**, 115314.
- 16 K. Kutsuki, T. Ono and K. Hirose, *Sci. Technol. Adv. Mater.*, 2007, **8**, 204.
- 17 B. E. Deal and C. R. Helms, *The Physics and Chemistry of SiO₂ and the Si-SiO₂ Interface*, Springer Science & Business Media, 2013, google-Books-ID: dg73BwAAQBAJ.
- 18 P. F. Satterthwaite, A. G. Scheuermann, P. K. Hurley, C. E. D. Chidsey and P. C. McIntyre, *ACS Appl. Mater. Interfaces*, 2016, **8**, 13140.
- 19 A. Bongiorno, A. Pasquarello, M. S. Hybertsen and L. C. Feldman, *Phys. Rev. Lett.*, 2003, **90**, 186101.
- 20 F. Rochet, C. Poncey, G. Dufour, H. Roulet, C. Guillot and F. Sirotti, *J. Non-Cryst. Solids*, 1997, **216**, 148.
- 21 F. J. Himpsel, F. R. McFeely, A. Taleb-Ibrahimi, J. A. Yarmoff and G. Hollinger, *Phys. Rev. B: Condens. Matter Mater. Phys.*, 1988, **38**, 6084.
- 22 K. Kimura and K. Nakajima, *Appl. Surf. Sci.*, 2003, **216**, 283.
- 23 N. Awaji, *Jpn. J. Appl. Phys.*, 1996, **35**, L67.

- 24 T. Suwa, A. Teramoto, K. Nagata, A. Ogura, H. Nohira, T. Muro, T. Kinoshita, S. Sugawa, T. Ohmi and T. Hattori, *Microelectron. Eng.*, 2013, **109**, 197.
- 25 J. H. Oh, H. W. Yeom, Y. Hagimoto, K. Ono, M. Oshima, N. Hirashita, M. Nywa, A. Toriumi and A. Kakizaki, *Phys. Rev. B: Condens. Matter Mater. Phys.*, 2001, **63**, 205310.
- 26 G. Lucovsky and J. C. Phillips, *J. Phys.: Condens. Matter*, 2004, **16**, S5139.
- 27 A. C. T. van Duin, A. Strachan, S. Stewman, Q. Zhang, X. Xu and W. A. Goddard, *J. Phys. Chem. A*, 2003, **107**, 3803.
- 28 K.-O. Ng and D. Vanderbilt, *Phys. Rev. B: Condens. Matter Mater. Phys.*, 1999, **59**, 10132.
- 29 S. Lee, R. J. Bondi and G. S. Hwang, *J. Appl. Phys.*, 2011, **109**, 113519.
- 30 S. von Alftthan, A. Kuronen and K. Kaski, *Phys. Rev. B: Condens. Matter Mater. Phys.*, 2003, **68**, 073203.
- 31 T. Anh Pham, T. Li, H.-V. Nguyen, S. Shankar, F. Gygi and G. Galli, *Appl. Phys. Lett.*, 2013, **102**, 241603.
- 32 A. Alkauskas, P. Broqvist, F. Devynck and A. Pasquarello, *Phys. Rev. Lett.*, 2008, **101**, 106802.
- 33 B. R. Tuttle, *Phys. Rev. B: Condens. Matter Mater. Phys.*, 2004, **70**, 125322.
- 34 Y. Tu, J. Tersoff, G. Grinstein and D. Vanderbilt, *Phys. Rev. Lett.*, 1998, **81**, 4899.
- 35 H. H. Pham, G. T. Barkema and L.-W. Wang, *Phys. Chem. Chem. Phys.*, 2015, **17**, 26270.
- 36 N. Mousseau and G. T. Barkema, *J. Phys.: Condens. Matter*, 2004, **16**, S5183.
- 37 L. Kong and L. J. Lewis, *Phys. Rev. B: Condens. Matter Mater. Phys.*, 2008, **77**, 085204.
- 38 J. Tersoff, *Phys. Rev. B: Condens. Matter Mater. Phys.*, 1988, **38**, 9902.
- 39 J. Tersoff, *Phys. Rev. B: Condens. Matter Mater. Phys.*, 1989, **39**, 5566.
- 40 S. R. Billeter, A. Curioni, D. Fischer and W. Andreoni, *Phys. Rev. B: Condens. Matter Mater. Phys.*, 2006, **73**, 155329.
- 41 J. Yu, S. B. Sinnott and S. R. Phillpot, *Phys. Rev. B: Condens. Matter Mater. Phys.*, 2007, **75**, 085311.
- 42 A. Yasukawa, *JSME Int. J., Ser. A*, 1996, **39**, 313.
- 43 T. Watanabe, H. Fujiwara, H. Noguchi, T. Hoshino and I. Ohdomari, *Jpn. J. Appl. Phys.*, 1999, **38**, L366.
- 44 Y. Tu and J. Tersoff, *Phys. Rev. Lett.*, 2000, **84**, 4393.
- 45 A. C. T. van Duin, A. Strachan, S. Stewman, Q. Zhang, X. Xu and W. A. Goddard, *J. Phys. Chem. A*, 2003, **107**, 3803.
- 46 G. Kovacevic and B. Pivac, *J. Appl. Phys.*, 2014, **115**, 043531.
- 47 W. Jia, Z. Cao, L. Wang, J. Fu, X. Chi, W. Gao and L.-W. Wang, *Comput. Phys. Commun.*, 2013, **184**, 9.
- 48 W. Jia, J. Fu, Z. Cao, L. Wang, X. Chi, W. Gao and L.-W. Wang, *J. Comput. Phys.*, 2013, **251**, 102.
- 49 J. P. Perdew, K. Burke and M. Ernzerhof, *Phys. Rev. Lett.*, 1996, **77**, 3865.
- 50 P. Giannozzi, S. Baroni, N. Bonini, M. Calandra, R. Car, C. Cavazzoni, D. Ceresoli, G. L. Chiarotti, M. Cococcioni, I. Dabo, A. D. Corso, S. de Gironcoli, S. Fabris, G. Fratesi, R. Gebauer, U. Gerstmann, C. Gouguassis, A. Kokalj, M. Lazzeri, L. Martin-Samos, N. Marzari, F. Mauri, R. Mazzarello, S. Paolini, A. Pasquarello, L. Paulatto, C. Sbraccia, S. Scandolo, G. Sclauzero, A. P. Seitsonen, A. Smogunov, P. Umari and R. M. Wentzcovitch, *J. Phys.: Condens. Matter*, 2009, **21**, 395502.
- 51 D. R. Hamann, *Phys. Rev. B: Condens. Matter Mater. Phys.*, 2013, **88**, 085117.
- 52 A. Alkauskas, P. Broqvist, F. Devynck and A. Pasquarello, *Phys. Rev. Lett.*, 2008, **101**, 106802.
- 53 J. H. Skone, M. Govoni and G. Galli, *Phys. Rev. B: Condens. Matter Mater. Phys.*, 2014, **89**, 195112.
- 54 S. Susman, K. J. Volin, D. L. Price, M. Grimsditch, J. P. Rino, R. K. Kalia, P. Vashishta, G. Gwanmesia, Y. Wang and R. C. Liebermann, *Phys. Rev. B: Condens. Matter Mater. Phys.*, 1991, **43**, 1194.
- 55 K. Laaziri, S. Kycia, S. Roorda, M. Chicoine, J. L. Robertson, J. Wang and S. C. Moss, *Phys. Rev. B: Condens. Matter Mater. Phys.*, 1999, **60**, 13520.
- 56 V. V. Afanas'ev, M. Houssa, A. Stesmans and M. M. Heyns, *Appl. Phys. Lett.*, 2001, **78**, 3073.
- 57 J. W. Keister, J. E. Rowe, J. J. Kolodziej, H. Niimi, T. E. Maday and G. Lucovsky, *J. Vac. Sci. Technol., B: Microelectron. Nanometer Struct.–Process., Meas., Phenom.*, 1999, **17**, 1831.